Supporting information

Self-Assembled Porphyrin Nanofiber Membrane-Decorated Alumina Channels for Enhanced Photoelectric Response

Dan Zhang, [†,⊥] Shuqi Zhou, [†,⊥] You Liu,[†] Xia Fan,[*,†] Mingliang Zhang,[*,‡,§] Jin Zhai[†] and Lei Jiang[†]

[†]Key Laboratory of Bio-Inspired Smart Interfacial Science and Technology of the Ministry of Education, School of Chemistry, Beihang University, Beijing 100083, People's Republic of China
[‡]Engineering Research Center for Semiconductor Integrated Technology, Institute of Semiconductors, Chinese Academy of Sciences, Beijing 100083, People's Republic of China
[§]College of Materials Science and Optoelectronic Technology, University of Chinese Academy of Sciences, Beijing 101408, People's Republic of China

E-mail: fanxia@buaa.edu.cn, zhangml@semi.ac.cn

Figure S1. The DLP device;
Figure S2. Schematic illustration of the process of heterogeneous TPPS/Al_2O_3 nanochannel formation with varying assembly times;
Figure S3. Schematic diagram of the custom-designed electrochemical cell device used for measuring the ionic transportation properties;
Figure S4. High-magnification SEM image of tip channels and low-magnification cross-sectional SEM image of hourglass-shaped Al_2O_3 nanochannels;
Figure S5. Image of the top surface of heterogeneous TPPS/Al_2O_3 nanochannels with varying assembly times;
Figure S6. UV-Vis absorption spectra of naked Al_2O_3 nanochannels and heterogeneous TPPS/Al_2O_3 nanochannels;
Figure S7. TEM images of TPPS nanofibers removed from the Al_2O_3 surface after different assembly times;
Figure S8. SEM images of the top surface flat and after tilting 30 degrees and the side view of TPPS/Al_2O_3 heterogeneous nanochannels with other specific assembly durations;
Figure S9. SEM images of other representative positions of the TPPS/Al_2O_3 heterogeneous nanochannels;
Figure S10. Cross-sectional fluorescence microscopy images of heterogeneous TPPS/Al_2O_3 nanochannels with different assembly times;
Figure S11. Fluorescence spectra of heterogeneous TPPS/Al_2O_3 nanochannels with different assembly times;
Figure S12. Schematic diagram of possible mechanism of membrane self-assembly on the top surface of Al_2O_3 membrane;
Figure S13. SEM images and photographs of the top and bottom surfaces and cross-sectional fluorescence images of cylindrical Al_2O_3 nanochannels;
Figure S14. *I-V* curves and rectification ratio of heterogeneous TPPS/Al_2O_3 nanochannels for various electrolyte concentrations;
Figure S15. *I-V* curves of hourglass-shaped Al_2O_3 nanochannels and heterogeneous TPPS/Al_2O_3 nanochannels under alternating illumination;
Figure S16. *I-t* curves of heterogeneous TPPS/Al_2O_3 nanochannels under alternating illumination comparable to sunlight in intensity.

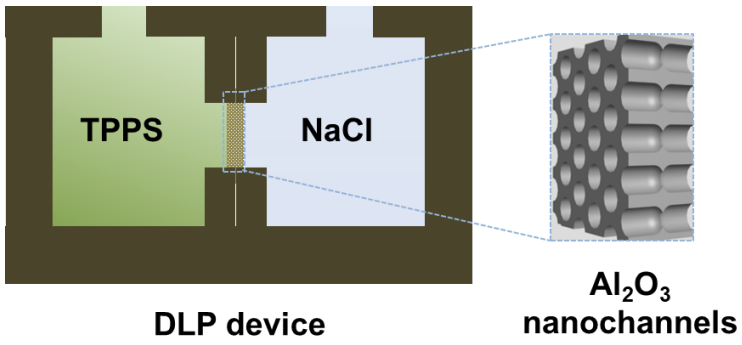

Figure S1. The DLP device, in which hourglass-shaped alumina nanochannels were mounted between the two halves of the homemade electrochemical cell. One half-cell was filled with aqueous TPPS solution, while the other half-cell was filled with sodium chloride solution.

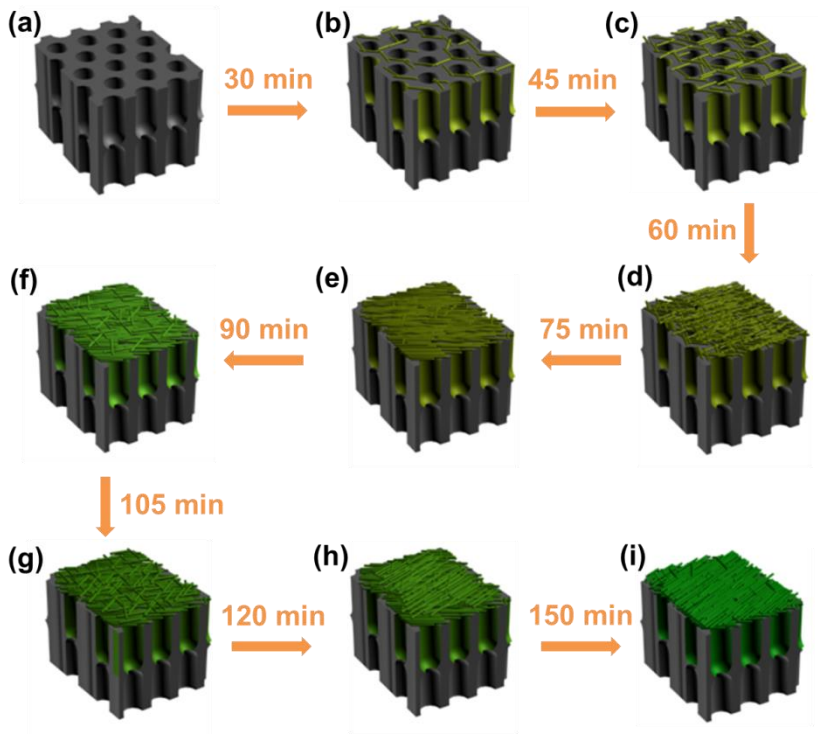

Figure S2. Schematic illustration of the heterogeneous TPPS/Al_2O_3 nanochannel formation process with assembly times of (a) 0, (b) 30, (c) 45, (d) 60, (e) 75, (f) 90, (g) 105, (h) 120, and (i) 150 min. With increasing time, the number, length and thickness of the TPPS nanofibers deposited on the top surface of the Al_2O_3 membrane gradually increased, and the pores of the top side of the Al_2O_3 nanochannels were sheltered more. Meanwhile, the orientation of these nanofibers gradually changed from disordered to ordered, and ultimately, a uniform membrane was formed. However, the nanofibers are not observed on the bottom of these heterogeneous nanochannels.

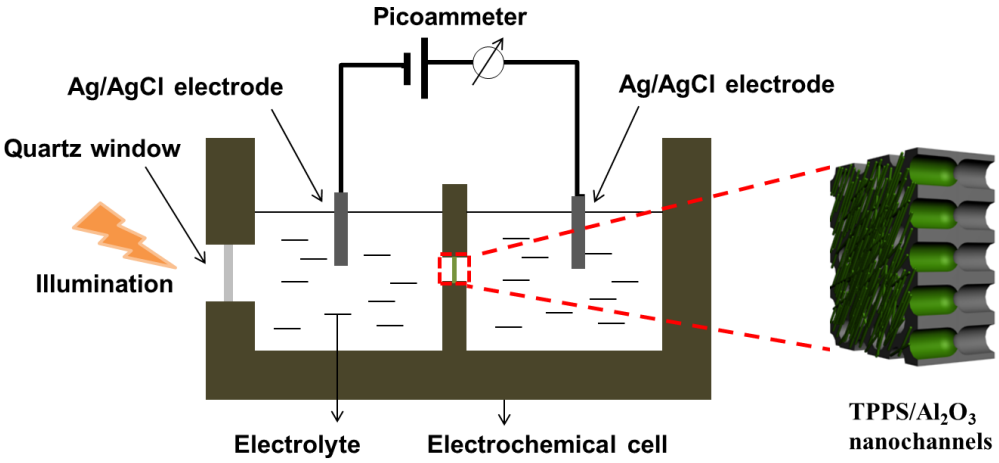

Figure S3. Schematic diagram of the custom-designed electrochemical cell device with a quartz window used to measure the ionic transportation properties of the TPPS/Al_2O_3 heterogeneous nanochannels. The current-voltage (*I*-*V*) measurements were performed at KCl electrolyte concentrations ranging from 0.1 to 100 mM or with and without illumination at 10 mM KCl.

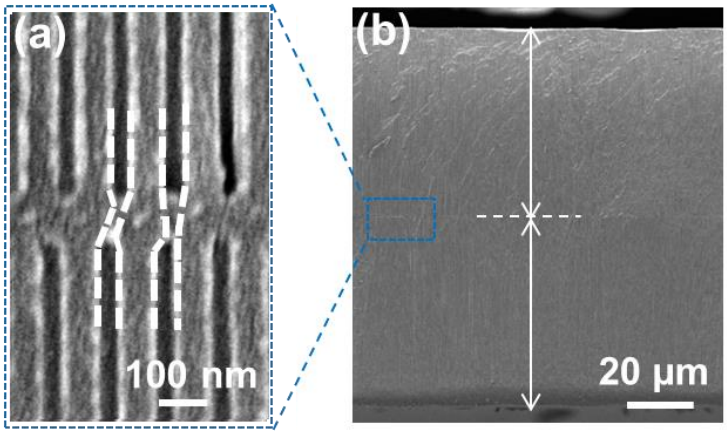

Figure S4. (a) High-magnification SEM image of tip channels and (b) low-magnification cross-sectional SEM image of hourglass-shaped Al_2O_3 nanochannels. The membrane thickness was approximately 100 μm and the diameter of tip channel in a weak boundary between the sides of the nanochannels was approximately 10 nm.

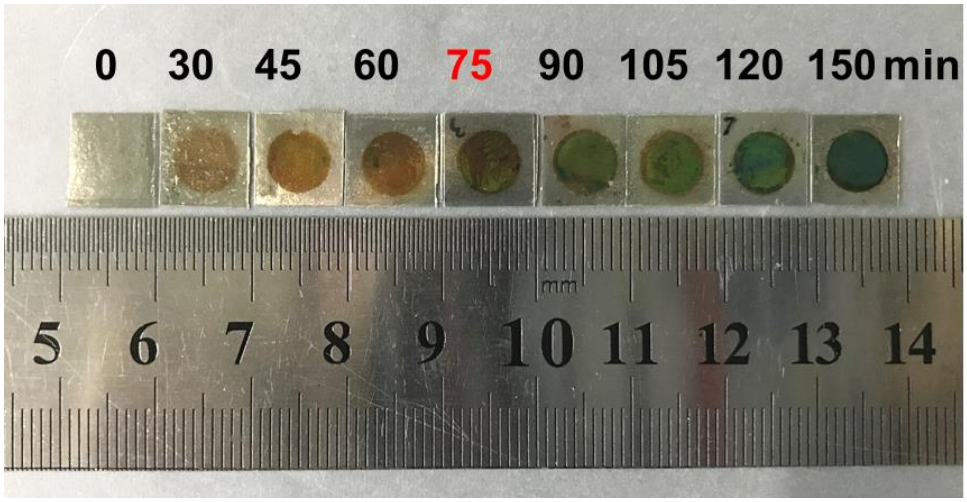

Figure S5. Photograph of the top surface of heterogeneous TPPS/Al_2O_3 nanochannels with assembly times of 0, 30, 45, 60, 75, 90, 105, 120, and 150 min. The naked Al_2O_3 nanochannels were semitransparent. After the deposition of TPPS molecules onto the Al_2O_3 nanochannels, the heterogeneous nanochannel membranes changed from yellow-green to dark-green from 30 to 150 min, with the color transition observed at 75 min. Thus, more and longer nanofibers formed on the surface of the Al_2O_3 membrane.

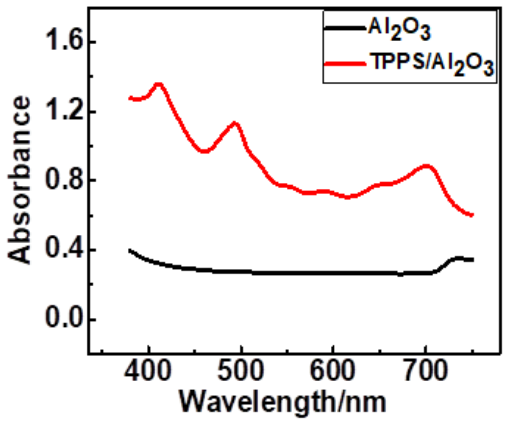

Figure S6. UV-vis absorption spectra of naked hourglass-shaped Al_2O_3 nanochannels (black curve) and heterogeneous TPPS/Al_2O_3 nanochannels with an assembly time of 75 min (red curve). New absorption bands at approximately 493 and 702 nm appeared for the heterogeneous nanochannels, and these were considered to be the characteristic peaks of the TPPS aggregation state.

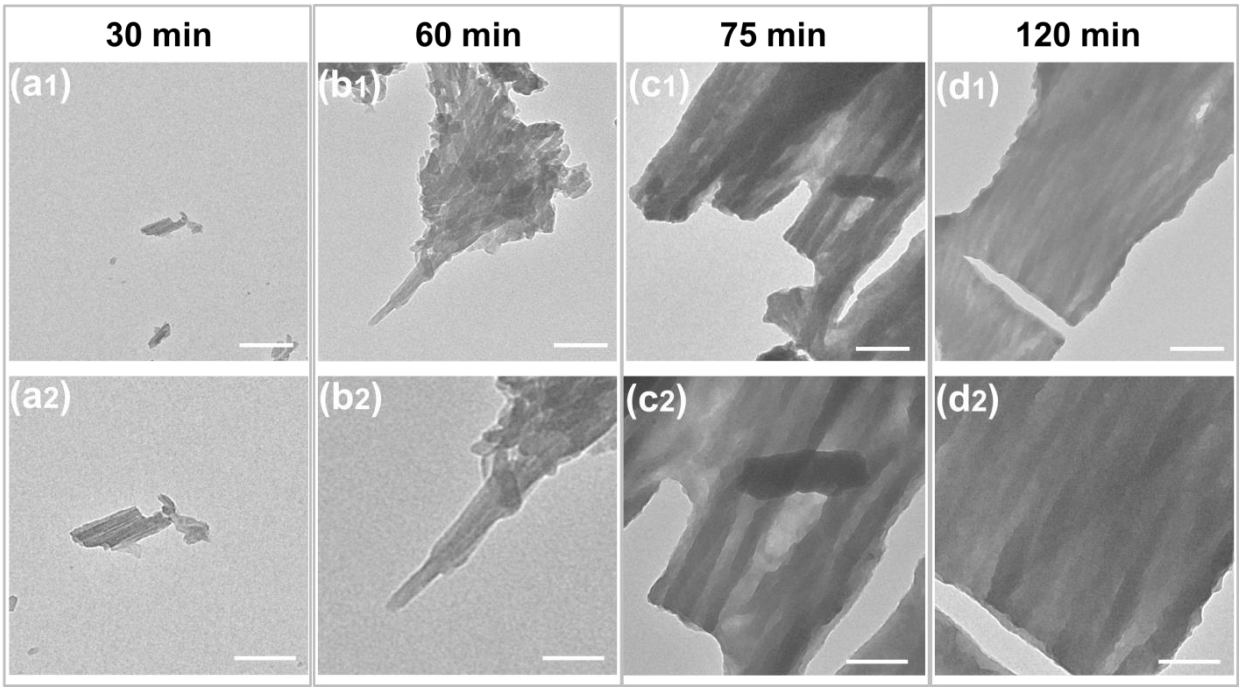

Figure S7. TEM images of TPPS nanofibers removed from the Al_2O_3 surface after assembly times of (a) 30, (b) 60, (c) 75, and (d) 120 min. Scale bars: 500 nm (a1-d1) and 200 nm (a2-d2).

The microscopic morphology of TPPS nanofibers was investigated by TEM. When the assembly time was 30 min, nanofibers between 200-300 nm in length were observed. When the time was 60 min, the length of the TPPS nanofibers increased. After 75 min, the network formed by the TPPS nanofibers constituted a thinner ordered membrane, and the length of nanofibers increased to 1 μm. The aggregated nanofibers become thicker and tighter when the assembly time was 120 min. Therefore, as the assembly time increased, the formed TPPS fibers became longer, and the number increased. Some fibers even joined together and tended to form ordered membranes.

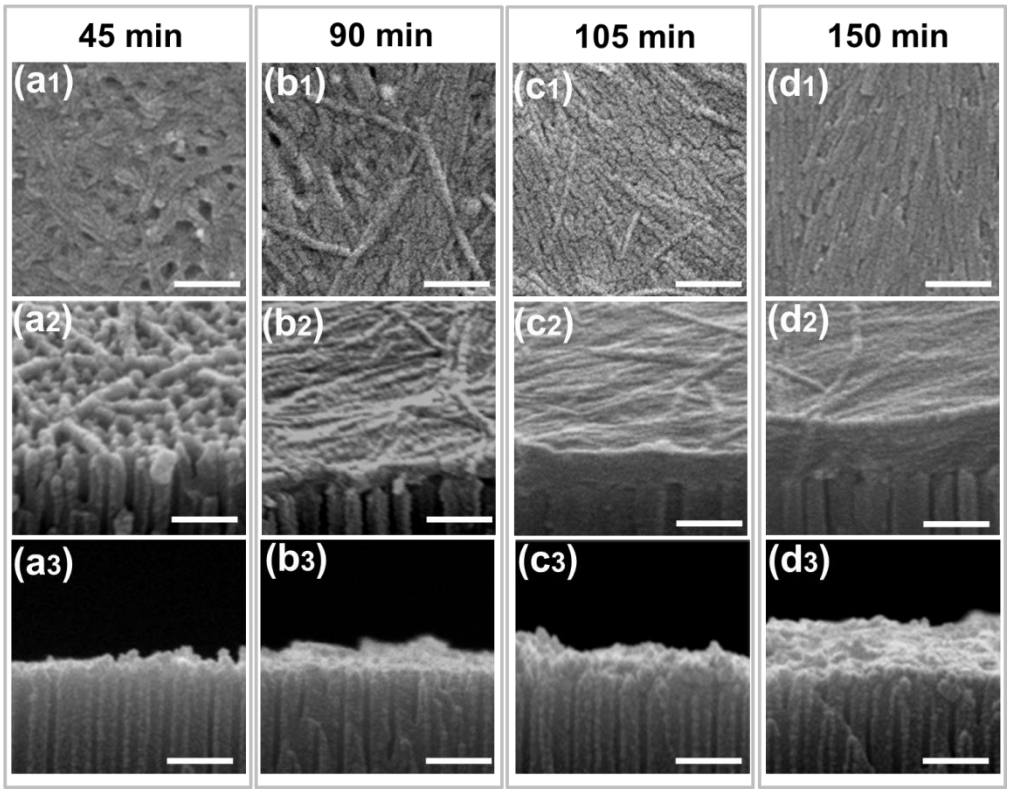

Figure S8. SEM images of the top surface flat and after tilting 30° , and the side view of TPPS/Al_2O_3 heterogeneous nanochannels with assembly times of (a1-a3) 45, (b1-b3) 90, (c1-c3) 105, and (d1-d3) 150 min. Scale bars: 300 nm.

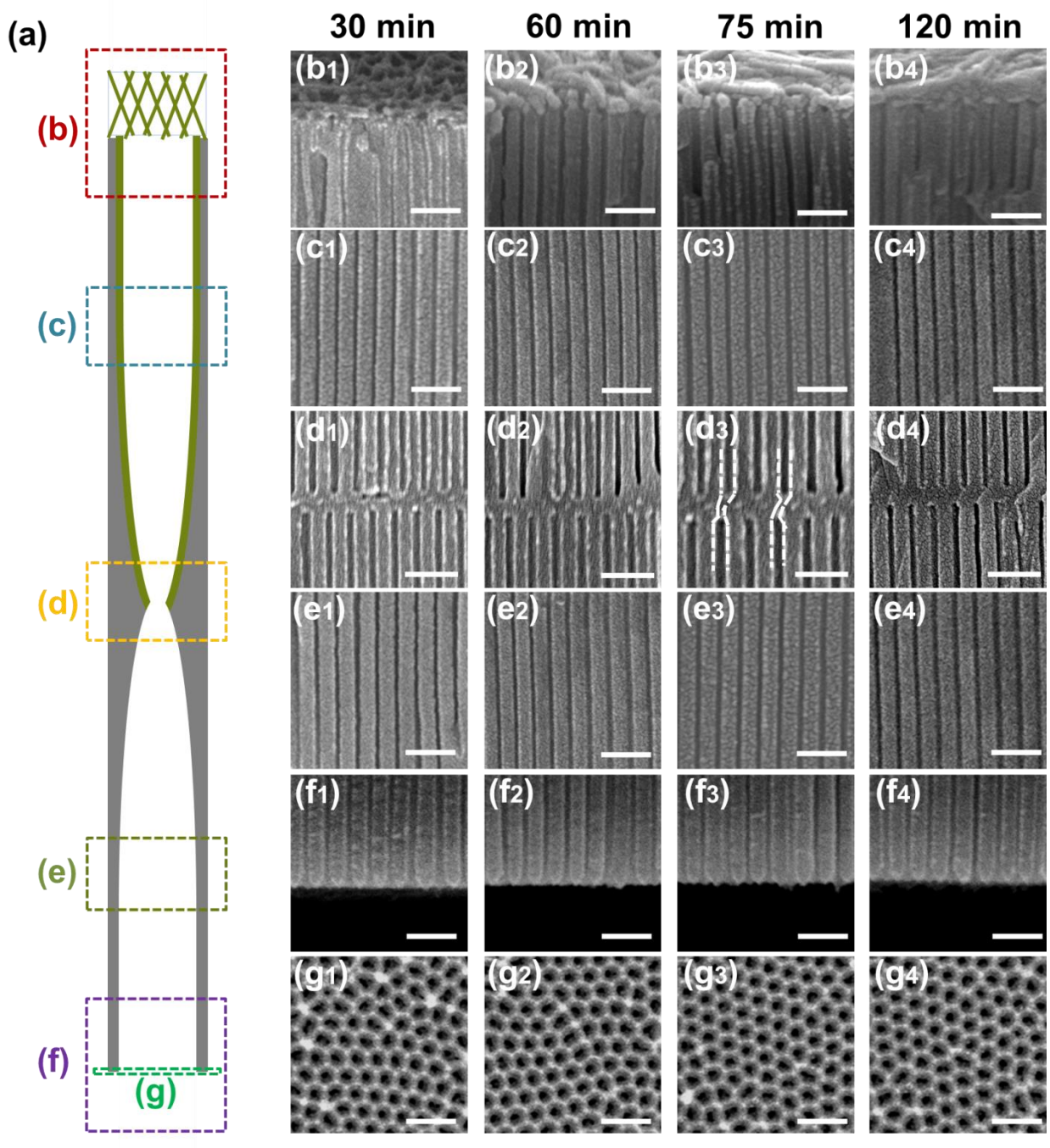

Figure S9. (a) Schematic illustration of single nanochannel belonging to porous heterogeneous TPPS/Al_2O_3 nanochannels. The SEM images of (b) the top surface after tilting 30 degrees, the side views including (c) the top side channels, (d) the tip channels, (e) the bottom side channels, and (f) the bottom entrance, and (g) the bottom surface of TPPS/Al_2O_3 heterogeneous nanochannels with assembly times of 30, 60, 75, and 120 min. Scale bars: 300 nm.

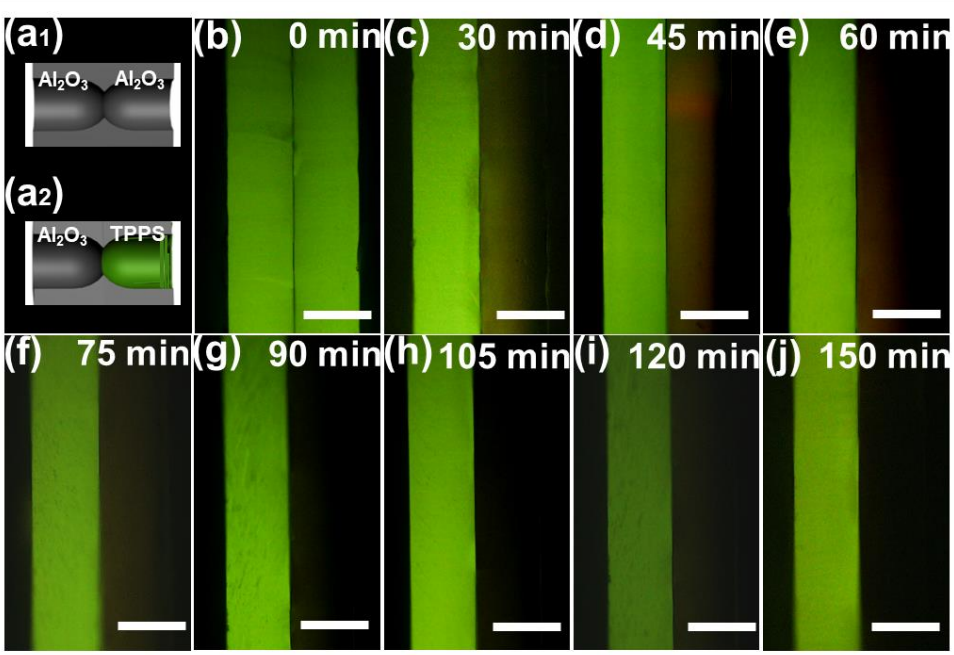

Figure S10. Schematic diagrams of a single nanochannel without self-assembled TPPS (a1) and with self-assembled TPPS (a2) on only one side of the hourglass-shaped nanochannels. Cross-sectional fluorescence images of heterogeneous TPPS/Al_2O_3 nanochannels obtained with assembly times of (b) 0, (c) 30, (d) 45, (e) 60, (g) 75, (g) 90, (h) 105, (i) 120, and (j) 150 min. Stronger contrast was observed between the two segments of the heterogeneous nanochannels (Figure S10c-j) than those of the naked Al_2O_3 nanochannels (Figure S10b), indicating occurrence of the molecular modification at the inner wall of one side of the Al_2O_3 nanochannels. The longer the assembly time, the darker the color of the TPPS-modified side, *i.e.*, over time, more TPPS molecules were deposited on the inner walls of the Al_2O_3 nanochannels. Scale bars: 50 μm.

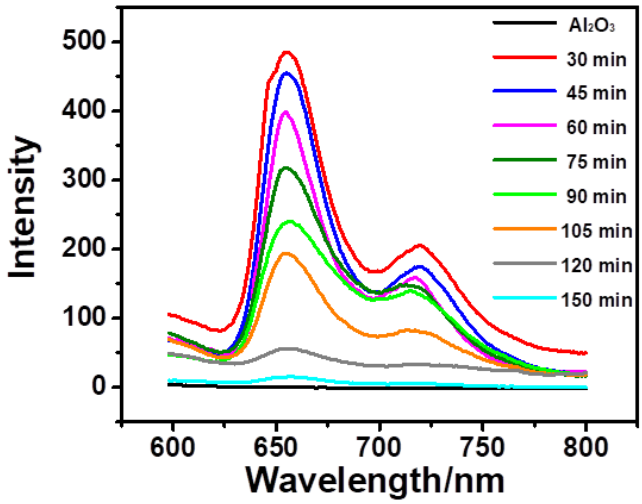

Figure S11. Fluorescence spectra of the heterogeneous TPPS/Al_2O_3 nanochannels with different assembly times of 0, 30, 45, 60, 75, 90, 105, 120, and 150 min. The excitation wavelength was 420 nm, and the scanning range of the emission wavelength was from 470 to 800 nm. The two emission peaks at approximately 653 and 717 nm were attributed to the transition of the first excitation singlet state S_1 to S_0 in TPPS. The fluorescence intensity decreased with increasing assembly time due to the aggregation of TPPS fibers resulting in quenching of the fluorescence of TPPS with a high quantity and density. [1, 2]

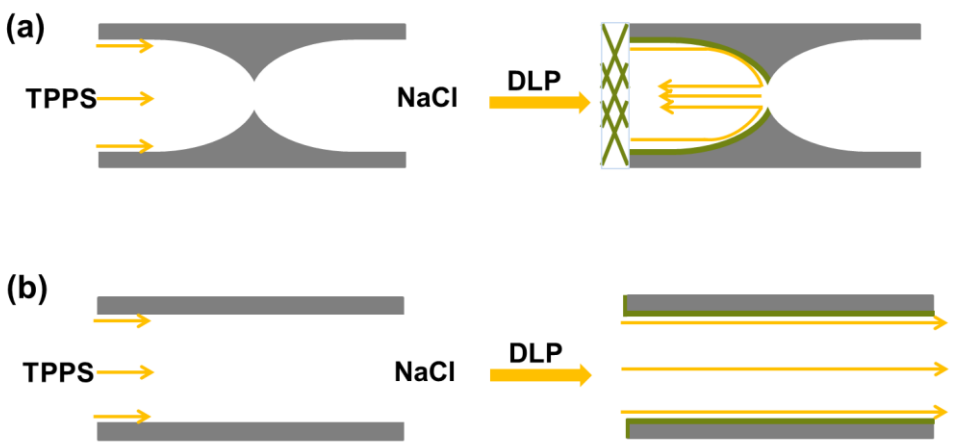

Figure S12. Schematic diagram of (a) the TPPS nanofiber membrane formed on the top surface membrane of hourglass-shaped Al_2O_3 nanochannels using the DLP method, in which the TPPS solution diffuses and modifies the inner wall of the Al_2O_3 nanochannels. As the TPPS aggregates cannot pass the Al_2O_3 tip barriers, they return, which increases the concentration of TPPS molecules and further promotes their self-assembly to effectively form a nanofiber membrane on one side of the Al_2O_3 nanochannels. (b) The TPPS nanofiber membrane cannot be formed on the top surface of cylindrical Al_2O_3 nanochannels using the DLP method, as most of the TPPS molecules pass directly through the channels (Figure S12b) and few molecules modify the surface of the channel.

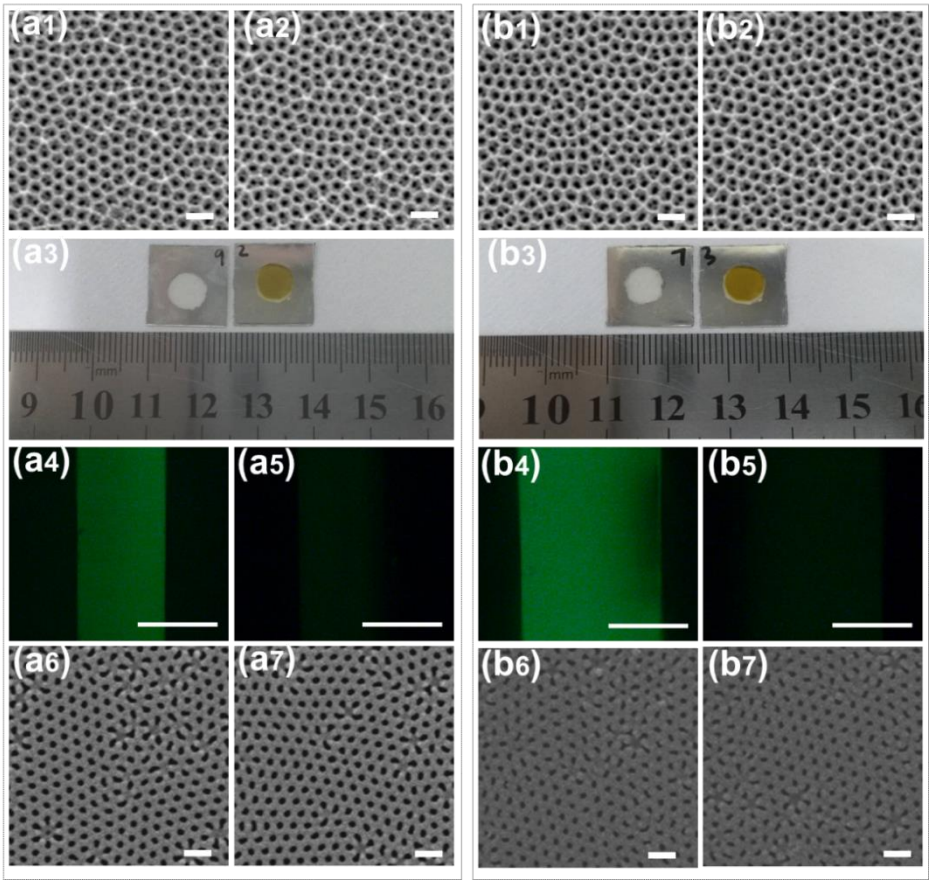

Figure S13. SEM images and photographs of the top surface and bottom surface and cross-sectional fluorescence images of cylindrical Al_2O_3 nanochannels with a membrane thickness of 50 μm (a) and 100 μm (b) before (a1, a4, a6, b1, b4, and b6) and after (a2, a5, a7, b2, b5, and b7) TPPS modification (time 75 min). No TPPS aggregates were observed, and only the TPPS molecular modification occurred. Scale bars: 300 nm (a1, a2, a6, a7, b1, b2, b6, and b7) and 50 μm (a4, a5, b4, and b5).

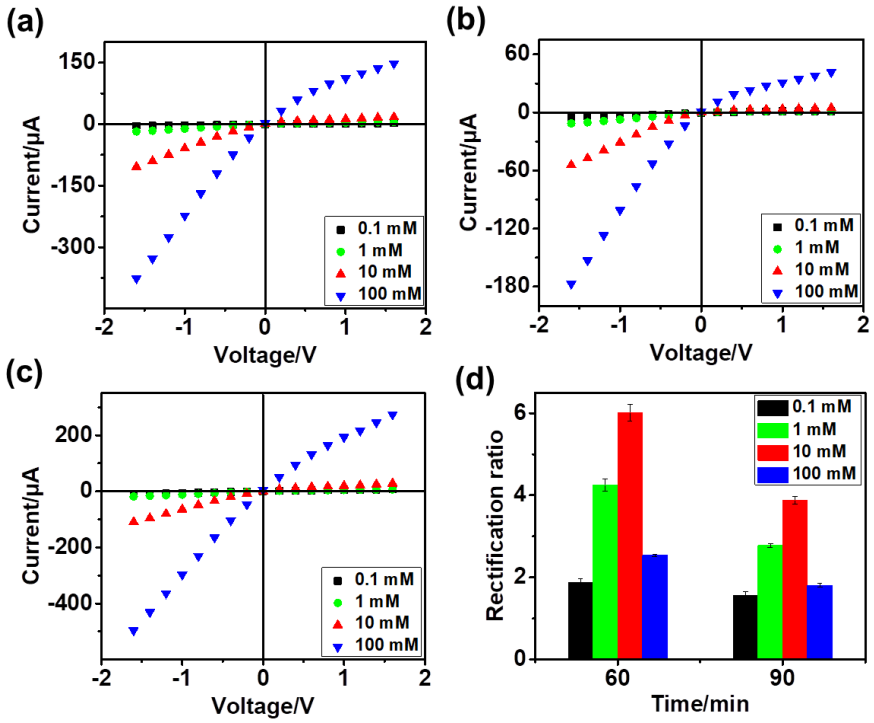

Figure S14. *I-V* curves of heterogeneous TPPS/Al_2O_3 nanochannels with assembly times of (a) 60 min, (b) 75 min, and (c) 90 min under varying electrolyte concentrations, in which the ionic current increased with electrolyte concentration. (d) Changes in the rectification ratio change with electrolyte concentration for assembly times of 60 and 90 min. The rectification ratio for both 60 and 90 min first increased and then decreased with increasing electrolyte concentration, reaching a maximum value at 10 mM.

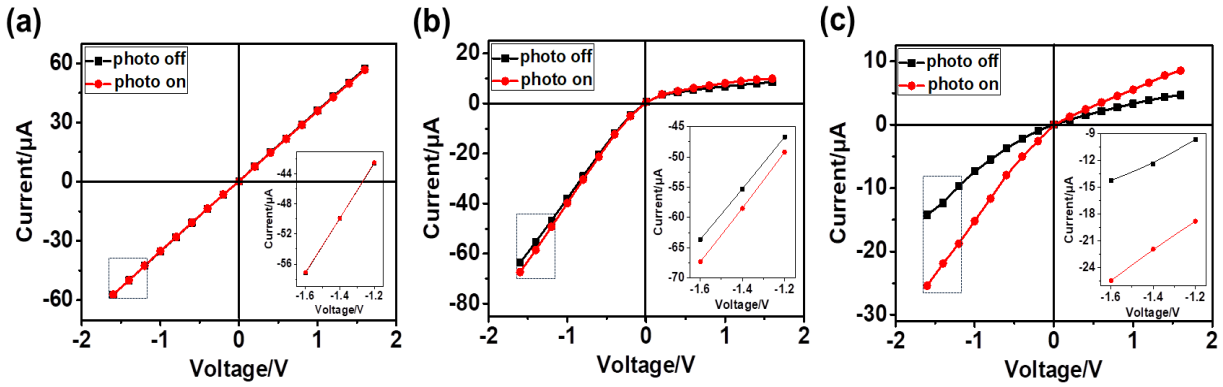

Figure S15. *I-V* curves of (a) hourglass-shaped Al_2O_3 nanochannels and heterogeneous TPPS/Al_2O_3 nanochannels with an assembly time of (b) 60 and (c) 90 min with and without illumination. The insets illustrate the region corresponding to the dotted line box. Naked Al_2O_3 nanochannels showed no photoresponse. The responsive current of the heterogeneous nanochannels with assembly times of 60 and 90 min at -1.6 V was 3.7 and 11.2 μA, respectively. In addition, the corresponding currents at 1.6 V are 1.4 and 3.8 μA, respectively.

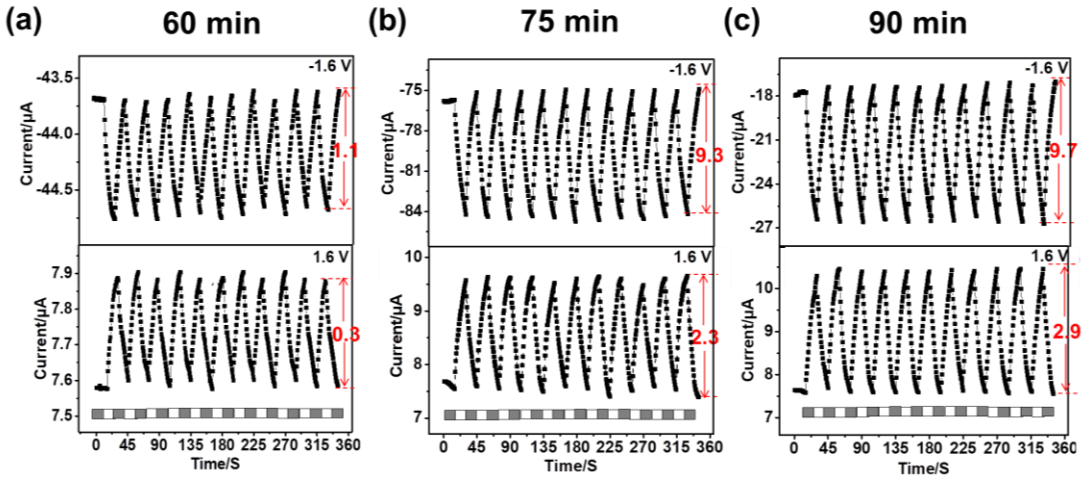

Figure S16. *I-t* curves of heterogeneous TPPS/Al_2O_3 nanochannels with assembly times of (a) 60, (b) 75, and (c) 90 min with and without illumination at -1.6 (top) and 1.6 V (bottom). The 12 cycles of alternating illumination showed that the photoswitching property of the heterogeneous TPPS/Al_2O_3 nanochannels has good reversibility.

Under alternating illumination, photoswitching can be achieved with heterogeneous TPPS/Al_2O_3 nanochannels with assembly times of 60, 75, and 90 min. When the illumination is switched on and off, the ionic current increases and decreases alternately. The photoresponse of ion transport through heterogeneous nanochannels showed good reversibility and stability. As illustrated in Figure S16, the responsive current of heterogeneous nanochannels with assembly times of 60, 75, and 90 min at -1.6 V was 1.1, 9.3, and 9.7 μA, respectively, and the corresponding current at 1.6 V was 0.3, 2.3, and 2.9 μA, further confirming that with longer assembly times, the photoresponse current increases.

References:

[1] Chen, Y.; Zheng, M.; Xiao, Y.; Dong, H.; Zhang, H.; Zhuang, J.; Hu, H.; Lei, B.; Liu, Y. A Self-Quenching-Resistant Carbon-Dot Powder with Tunable Solid-State Fluorescence and Construction of Dual-Fluorescence Morphologies for White Light-Emission. *Adv. Mater.* **2016**, *28*, 312-318.

[2] Song, P.; Xiang, Y.; Wei, R.; Tong, A. A Fluorescent Chemosensor for Cu^{2+} Detection in Solution Based on Aggregation-Induced Emission and Its Application in Fabricating Cu^{2+} Test Papers. *J. Lumin.* **2014**, *153*, 215-220.